Structural snapshots of phenuivirus cap-snatching and transcription

Harry M Williams, Sigurdur R Thorkelsson, Dominik Vogel, Carola Busch, Morlin Milewski, Stephen Cusack, Kay Grünewald, Emmanuelle R Quemin, Maria Rosenthal

Nucleic Acids Research, 2024, **52**, 6049–6065
https://doi.org/10.1093/nar/gkae330
Advance access publication date: 6 May 2024
Structural Biology

Structural snapshots of phenuivirus cap-snatching and transcription

Harry M. Williams [1,2,3], Sigurdur R. Thorkelsson[2,3,4], Dominik Vogel [1], Carola Busch[1], Morlin Milewski[1], Stephen Cusack [5], Kay Grünewald[2,3,4], Emmanuelle R.J. Quemin[2,3,6] and Maria Rosenthal [1,2,7,*]

[1]Bernhard Nocht Institute for Tropical Medicine (BNITM), Hamburg, Germany
[2]Centre for Structural Systems Biology (CSSB), Hamburg, Germany
[3]Leibniz Institute of Virology, Hamburg, Germany
[4]University of Hamburg, Hamburg, Germany
[5]European Molecular Biology Laboratory, Grenoble, France
[6]Department of Virology, Institute for Integrative Biology of the Cell (I2BC), Centre National de la Recherche Scientifique (CNRS) UMR9198, Gif-sur-Yvette, France
[7]Fraunhofer Institute for Translational Medicine and Pharmacology (ITMP), Discovery Research ScreeningPort, Hamburg, Germany

[*]To whom correspondence should be addressed. Tel: +49 40 285380 930; Email: rosenthal@bnitm.de
Present address: Sigurdur R. Thorkelsson, MRC Laboratory of Molecular Biology (LMB), Cambridge, UK.

Abstract

Severe fever with thrombocytopenia syndrome virus (SFTSV) is a human pathogen that is now endemic to several East Asian countries. The viral large (L) protein catalyzes viral transcription by stealing host mRNA caps via a process known as cap-snatching. Here, we establish an *in vitro* cap-snatching assay and present three high-quality electron cryo-microscopy (cryo-EM) structures of the SFTSV L protein in biologically relevant, transcription-specific states. In a priming-state structure, we show capped RNA bound to the L protein cap-binding domain (CBD). The L protein conformation in this priming structure is significantly different from published replication-state structures, in particular the N- and C-terminal domains. The capped-RNA is positioned in a way that it can feed directly into the RNA-dependent RNA polymerase (RdRp) ready for elongation. We also captured the L protein in an early-elongation state following primer-incorporation demonstrating that this priming conformation is retained at least in the very early stages of primer extension. This structural data is complemented by *in vitro* biochemical and cell-based assays. Together, these insights further our mechanistic understanding of how SFTSV and other bunyaviruses incorporate stolen host mRNA fragments into their viral transcripts thereby allowing the virus to hijack host cell translation machinery.

Graphical abstract

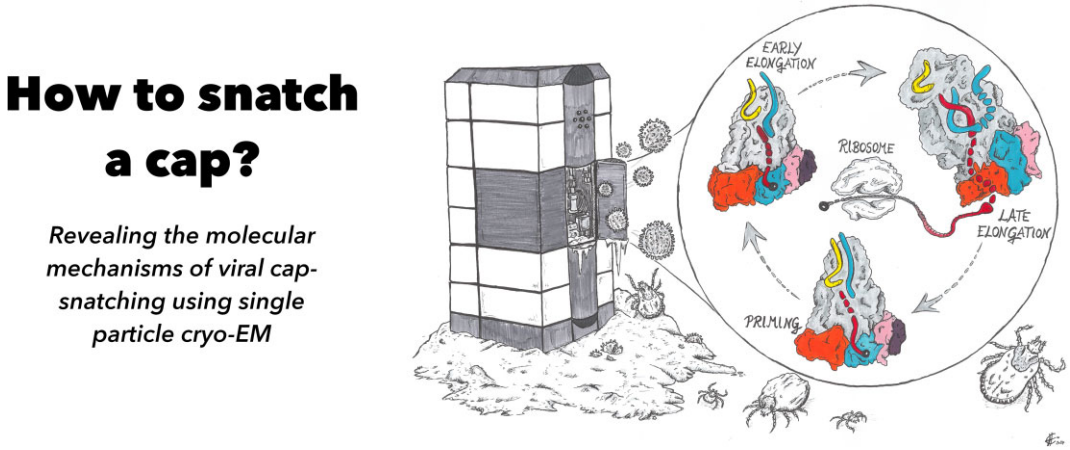

Introduction

Severe fever with thrombocytopenia syndrome virus (SFTSV) is a segmented negative-strand RNA virus in the order *Bunyavirales*, family *Phenuiviridae* (1). SFTSV has been identified in several East Asian countries, including China, Japan, and South Korea to cause human disease (2–7). Transmitted by ticks, SFTSV is known to infect a range of domestic animals, like cats and dogs, as well as a wide variety of livestock such

Received: December 18, 2023. **Revised:** April 10, 2024. **Editorial Decision:** April 11, 2024. **Accepted:** April 19, 2024

as cows, chickens, sheep, and pigs (8–11). Although SFTSV is thought to be predominantly transmitted by tick bite, there is also some evidence of human-to-human transmission (12,13). For these reasons, SFTSV is considered a significant threat to global public health with no effective medical countermeasures available.

A key target for the development of new antiviral strategies is the bunyaviral large (L) protein, a multidomain and multifunctional protein essential for both viral genome replication and transcription processes (14). During infection, the negative-sense genomic viral RNA (vRNA) is first copied into a positive-sense complementary RNA (cRNA) intermediate (15). This cRNA is then used as a template to reproduce the negative-sense vRNA, ready for packaging into progeny virions (15). It has been shown for bunyaviruses that viral genome replication can be initiated *de novo* using two different mechanisms: either initiation happens terminally or a short primer is produced internally and subsequently realigned to the 3′ *via* a prime-and-realign mechanism (16–18). For SFTSV, biochemical data has yet to distinguish between the two scenarios; however, recent structural data addressing how the SFTSV L protein enables viral genome replication suggest a prime-and-realign mechanism is more likely (18,19). On the other hand, bunyavirus transcription is thought to be initiated *via* a process known as cap-snatching (20). Similar to influenza virus transcription, short fragments of 5′-capped host cell mRNAs are used by the L protein to prime the synthesis of viral mRNAs (20). This allows the virus to hijack the translation machinery of the infected host cell for the production of viral proteins. Therefore, viral transcription relies on the endonuclease (ENDO) and cap-binding domains (CBD) of the L proteins and the length of the '*stolen*' capped primers appears to be specific to individual bunyaviruses. For example, Lymphocytic Choriomeningitis virus (LCMV, family *Arenaviridae*) uses a relatively short 1–7 nt primer (21), whereas Rift Valley fever virus (RVFV, family *Phenuiviridae*) requires a longer primer in the range of 12–14 nts (22). Because of their importance in these processes, the isolated cap-binding and ENDO domains of several bunyaviruses have been investigated extensively by X-ray crystallography (18,23–31).

Recently, electron cryo-microscopy (cryo-EM) data from single-particle analysis have become available for several full-length bunyavirus L proteins in complex with viral RNA, including Lassa virus and Machupo virus (LASV and MACV, family *Arenaviridae*), La Crosse virus (LACV, family *Peribunyaviridae*), Sin Nombre Virus and Hantaan virus (SNV and HTNV, family *Hantaviridae*) (16,32–38). This structural data has provided key insights into how these molecular machines interact with the viral RNA promoter and undergo major conformational changes during viral genome replication (39). For SFTSV, high-resolution cryo-EM structures of the L protein in various functionally relevant states of the viral genome replication process, from pre-initiation to late-stage elongation, have also been published (19). This data revealed how the SFTSV L protein binds the 5′ viral RNA in a hook-like conformation and further showed how the 5′ and 3′ RNAs form a distal duplex structure positioning the 3′ RNA terminus in the RdRp active site ready for initiation (19). Further, we could show that at late-stage elongation the L protein core accommodates a 10-bp product-template duplex which splits at the bottom of the RdRp core. In this conformation, the template RNA then binds to a designated 3′ secondary binding site in a similar fashion to that seen for other negative-strand RNA viruses, including LASV and LACV L proteins as well as the influenza virus polymerase complex (19,32,33,40,41).

These insights notwithstanding, much still remains unknown, especially in relation to how the SFTSV L protein enables viral transcription. Specifically, how does the SFTSV CBD interact with and bind to capped-RNA? How does the L protein present bound capped-RNA fragments to the ENDO for cleavage? How does the L protein then incorporate the cleaved snatched capped-RNA fragment into progeny RNA? Finally, it is still very much an open question how different L protein functions are regulated during infection to switch between *de novo* replication and primed transcription.

To answer these questions, here we used a combination of biochemical *in vitro* assays and single particle cryo-EM to visualise and understand how the SFTSV L protein steals and then incorporates host mRNA fragments into their viral RNA. We establish an *in vitro* cap-snatching assay and present three cryo-EM structures of the SFTSV L protein captured during viral transcription. The data are refined to an overall resolution of 2.98–3.40 Å. This structural data is validated by a comprehensive mutational analysis in a cell-based mini-replicon system. Together, these insights further our understanding of how SFTSV and other bunyaviruses steal and incorporate host mRNA fragments into their viral RNA thereby allowing the virus to hijack the host cell translation machinery.

Materials and methods

Expression and purification of SFTSV L protein

The L gene of SFTSV AH 12 (accession no. HQ116417) containing a C-terminal StrepII-tag was chemically synthesized (Centic Biotech, Germany) and cloned into an altered pFastBacHT B vector (18). Point mutations (D112A) were introduced by mutagenic PCR to reduce the SFTSV L proteins intrinsic endonuclease activity (31). DH10EMBacY *Escherichia coli* cells were used to generate recombinant baculoviruses (42,43), which were subsequently used for L protein expression in Hi5 insect cells. The harvested Hi5 insect cells were resuspended in Buffer A (50 mM HEPES[NaOH] pH 7.0, 1 M NaCl, 10% [w/v] glycerol and 2 mM DTT), supplemented with 0.05% (v/v) Tween20 and protease inhibitors (cOmplete mini, Roche), lysed by sonication, and centrifuged twice (20 000 × g for 30 min at 4°C). The soluble protein fraction was loaded on Strep-TactinXT beads (IBA Lifesciences) and eluted with 50 mM Biotin (Applichem) in Buffer B (50 mM HEPES[NaOH] pH 7.0, 500 mM NaCl, 10% [w/v] glycerol and 2 mM DTT). L protein-containing fractions were pooled and diluted 1:1 with Buffer C (20 mM HEPES[NaOH] pH 7.0) before loading on a heparin column (HiTrap Heparin HP, Cytiva). Proteins were eluted with Buffer A and concentrated using centrifugal filter units (Amicon Ultra, 30 kDa MWCO). L proteins then used for single-particle cryo-EM were further purified by size-exclusion chromatography using a Superdex 200 column (Cytiva, formerly GE Life Sciences) in Buffer B. Purified L proteins were concentrated as described above, flash frozen in liquid nitrogen and stored at −80°C.

Polymerase assay

RNA preparation

Primer A-PP (1–24) and Primer B-PP (1–32) were chemically synthesized with a 5′ diphosphate modification (Chemgenes) (Supplementary Table S1). An N7-MeGppp (cap^0) was

introduced at the 5′ terminus of Primer A-PP (1–24) and Primer B-PP (1–32) using the ScriptCap m^7G Capping System (CELLSCRIPT) with 50 μg oligo, according to the manufacturer's standard protocol. After the addition of cold AmOAc (2.5 M) the capped RNA was precipitated overnight in EtOH (>99%) at −20°C, washed two times with EtOH (80%), dried and dissolved in DEPC treated H_2O at room temperature. The capped RNA was purified further by passing through a MicroSpin G-25 column, as per the manufacturer's instructions. This protocol was also used to produce the radiolabelled capped Primer A-PP (1–24) with the only difference between the replacement of '*cold*' GTP (that is to say, not radiolabelled) provided in the ScriptCap m^7G Capping System with radioactive [α]32P-GTP (Hartmann Analytic). Purification of the radiolabelled capped RNA proceeded similarly: after the addition of cold AmOAc (2.5 M) the capped RNA was precipitated overnight in EtOH (>99%) at −20°C, washed two times with EtOH (80%), dried and dissolved in DEPC treated H_2O at room temperature.

In vitro cap-snatching assay

For the *in vitro* cap-snatching assay, 0.8 μM of the wild-type SFTSV L protein was incubated sequentially with single-stranded L 5′ (1–20) RNA and single-stranded L 3′-6A (1–26) modified with 6 additional A bases, at a ×1.1 molar excess to the L protein in assay buffer (100 mM HEPES, 50 mM KCl, and 2 mM DTT, pH 7) on ice for 5 min (Supplementary Table S1). To this, either Primer A-PP (1–24) or Primer B-PP (1–32) was added to a final concentration of 4.5 μM and the reaction incubated on ice for additional 30 minutes. The reaction was started by the addition of NTPs (0.2 mM ATP/UTP/GTP, 0.1 mM CTP spiked with 166 nM 5 μCi [α]32P-CTP (Hartmann Analytic)) and $MgCl_2$ (final concentration 2.5 mM) in a final reaction volume of 10 μl. After incubation at 30°C for 1–60 min, the reaction was stopped by adding an equivalent volume of RNA loading buffer (98% formamide, 18 mM EDTA, 0.025 mM SDS, xylene cyanol and bromophenol blue) and heating the samples at 95°C for 5 min. Products were then separated by denaturing gel electrophoresis using 25% polyacrylamide 7 M urea gels and 0.5-fold Tris–borate–EDTA running buffer. Signals were visualised by phosphor screen autoradiography using a Typhoon FLA-7000 phosphorimager (Fujifilm) operated with the FLA-7000 software.

For the *in vitro* (radiolabelled capped RNA) cap-snatching assay, 0.8 μM of the wild-type SFTSV L protein was incubated sequentially with single-stranded L 5′ (1–20) RNA and single-stranded L 3′-6A (1–26) modified with 6 additional A bases, at a ×1.1 molar excess to the L protein in assay buffer (100 mM HEPES, 50 mM KCl, and 2 mM DTT, pH 7) on ice for 5 min (Supplementary Table S1). To this, a combination of '*cold*' (*i.e.*, not radiolabelled) and '*hot*' (*i.e.*, radiolabelled) Primer A-CAP was added to an approximate final concentration of 4.5 μM and the mix was incubated on ice for additional 30 min. The reaction was started by the addition of NTPs (50 nM ATP/UTP/GTP/CTP) and $MgCl_2$ (final concentration 2.5 mM) in a final reaction volume of 10 μl. After incubation at 30°C for 5–60 min, the reaction was stopped by adding an equivalent volume of RNA loading buffer (98% formamide, 18 mM EDTA, 0.025 mM SDS, xylene cyanol and bromophenol blue) and heating the samples at 95°C for 5 min. Products were then separated and visualised as outlined for the *in vitro* cap-snatching assay.

Rift Valley fever virus mini-replicon system

The experiments were performed using the RVFV mini-replicon system described previously (44). L genes were amplified using mutagenic PCR from a pCITE2a-L template to produce either wild-type or mutated L gene expression cassettes. PCR products were gel purified and quantified spectrophotometrically. All mutations were confirmed by sequencing of the PCR products. BSR-T7 cells were transfected per well of a 24 well plate with 250 ng of L gene PCR product, 500 ng of pCITE expressing NP, 750 ng of pCITE expressing the mini-genome RNA encoding Renilla luciferase (Ren-Luc), and 10 ng of pCITE expressing the firefly luciferase as an internal control. At 24 h post-transfection, either total cellular RNA was extracted for Northern blot analysis using an RNeasy Mini kit (Qiagen) or cells were lysed in 100 μl of passive lysis buffer (Promega) per well, and firefly luciferase and Ren-Luc activity quantified using the dual-luciferase reporter assay system (Promega). Ren-Luc levels were corrected with the firefly luciferase levels (resulting in standardised relative light units [sRLU]) to compensate for differences in transfection efficiency or cell density. Data were evaluated in Prism and are always presented as the mean of a given amount (n) of biological replicates as well as the respective standard deviation (SD).

Northern blot analysis

For the Northern blot analysis, 600–1000 ng of total cellular RNA was separated in a 1.5% agarose-formaldehyde gel and transferred onto a Roti-Nylon plus membrane (pore size 0.45 μM, Carl Roth). After UV cross-linking and methylene blue staining to visualize 28 S rRNA, the blots were hybridised with a 32P-labelled riboprobe targeting the Ren-Luc gene. Transcripts of the Ren-Luc gene and complementary replication intermediate RNA of the minigenome were visualised by autoradiography using a Typhoon FLA-7000 phosphorimager (Fujifilm) operated with the FLA-7000 software. Quantification of signals for antigenomic RNA and mRNA was done in Fiji. To confirm general expressability of the L protein mutants in BSR-T7 cells, the cells were transfected with 500 ng L gene PCR product expressing C-terminally 3xFLAG-tagged L protein mutants per well. Cells were additionally infected with Modified Vaccinia virus Ankara expressing a T7 RNA polymerase (MVA-T7) to boost the expression levels and, thereby facilitate detection by immunoblotting. At 24 h post-transfection, cells were lysed in 50 μl passive lysis buffer (Promega) per well. After cell lysis and separation in a 3–8% Tris-acetate polyacrylamide gel (Invitrogen), proteins were transferred to a nitrocellulose membrane (Cytiva). FLAG-tagged L protein mutants were detected using horseradish peroxidase-conjugated anti-FLAG M2 antibody (1:9000) (A8592; Sigma-Aldrich) and bands were visualised by chemiluminescence using Clarity Max Western ECL Substrate (Bio-Rad) and a FUSION SL image acquisition system (Vilber Lourmat). Although we include a fast green staining of the membranes as a loading control in the Supplementary data, we explicitly do not quantify bands corresponding to the L proteins on the western blots. These blots only serve to check for L protein expressability.

Sample preparation for cryo-EM

TRANSCRIPTION-PRIMING and TRANSCRIPTION-PRIMING (*in vitro*) structures

The SFTSV L protein at a concentration of 3 μM in assay buffer (100 mM HEPES, 50 mM KCl, 2.5 mM $MgCl_2$ and 2 mM DTT, pH 7) was mixed sequentially with single-stranded L 5′ (1–20) RNA and single-stranded L 3′-6A (1–26) RNA modified with six additional A bases, in a ×6 molar excess. Single-stranded, capped RNA (Primer C-CAP, 1–17, Supplementary Table S1) was then added and the L protein–RNA mixture incubated on ice for 30 min. After incubation at 30°C for 5 min, the sample was then centrifuged at 15 000 × g for 10 min at 4°C. Aliquots of 3 μl were applied to Quantifoil R 2/1 Au G200F4 grids, immediately blotted for 2 s, and plunge frozen into liquid ethane/propane cooled to liquid nitrogen temperature using a FEI Vitrobot Mark IV (4°C, 100% humidity, blotting force −10).

TRANSCRIPTION-EARLY-ELONGATION structure

The SFTSV L protein at a concentration of 3 μM in assay buffer (100 mM HEPES, 50 mM KCl, 2.5 mM $MgCl_2$ and 2 mM DTT, pH 7) was mixed sequentially with single-stranded L 5′ (1–20) RNA and single-stranded L 3′-mid AAA (1–20) RNA where nts 6 – 8 have been replaced by A's, in a ×1.1 molar excess. Single-stranded capped-RNA (Primer C-CAP, 1–17, Supplementary Table S1) was then added and the L protein–RNA mixture incubated on ice for 30 min, after which the reaction was initiated by addition of NTPs (0.63 mM ATP/CTP/GTP/UpNHpp (Jena Bioscience)). After incubation at 30°C for 2 h, the sample was then centrifuged at 15 000 × g for 10 min at 4°C. Aliquots of 3 μl were applied to Quantifoil R 2/1 Au G200F4 grids, immediately blotted for 2 s, and plunge frozen into liquid ethane/propane cooled to liquid nitrogen temperature using a FEI Vitrobot Mark IV (4°C, 100% humidity, blotting force −10).

Cryo-EM single-particle analysis

Data collection

Grids were loaded into a 300-kV Titan Krios transmission electron microscope (Thermo Fisher Scientific) equipped with a K3 direct electron detector and a post-column GIF BioQuantum energy filter (Gatan). Micrograph movies were typically collected using the EPU software (Thermo Fisher Scientific) at a nominal magnification of either 105 000× with a pixel size of 0.85 Å using a defocus range of –0.8 to –2.6 μm (TRANSCRIPTION-PRIMING and TRANSCRIPTION-PRIMING (*in vitro*) structures) or a nominal magnification of 130 000× with a pixel size of 0.67 Å using a defocus range of –0.8 to –2.4 μm (TRANSCRIPTION-EARLY-ELONGATION structure). The samples were exposed to a total dose of 50 electrons/$Å^2$. Recorded movie frames were fractionated into 50 frames. A summary of the key data collection statistics for the dataset used to determine each cryo-EM structure is provided in Supplementary Table S2.

Image processing

All movie frames were imported in RELION 4.0 (45) and motion corrected using its own implementation of MotionCor2 (46). Particles were picked automatically using the pre-trained BoxNet2Mask_20180918 model in Warp (47). Calculation of contrast transfer function (CTF) estimation and correction was done in RELION 4.0 with CTFFIND4 (48). Picked particles were extracted and processed in RELION 4.0. First, particles were subjected to 2D classification at 4× binned pixel size. Then, all non-junk particles were used for 3D classification in an iterative manner using a 40 Å low pass filtered map of the apo SFTSV L protein (PDB: 6Y6K) (18). Incomplete, low resolution or 3D classes containing damaged particles were excluded from further data analyses. The remaining particles were re-extracted with the original pixel size value for further 3D classification and refinement. The processing pipeline for each structure determination is given in Supplementary Figure S1 (TRANSCRIPTION-PRIMING and TRANSCRIPTION-PRIMING (*in vitro*) structures) and Supplementary Figure S2 (TRANSCRIPTION-EARLY-ELONGATION structure). All cryo-EM maps were CTF-refined and Bayesian-polished before final refinement in RELION 4.0. All final cryo-EM density maps were generated by post-processing in RELION 4.0. The resolutions of the cryo-EM density maps were estimated using the 0.143 gold standard Fourier Shell Correlation (FSC) cut-off. A summary of the key processing statistics for each cryo-EM structure determination is provided in Supplementary Table S2.

Model building, refinement and validation

The recently published SFTSV EARLY-ELONGATION structure (PDB: 8AS7) was used as the starting point for modelling of the structures published in this study (19). These initial models underwent iterative rounds of model building in Coot (49) followed by real-space refinement in Phenix (50). The comprehensive validation tool in Phenix was then used to assess model quality (50,51). Coordinates and EM maps are deposited in the PDB and EMDB databases, as indicated in Supplementary Table S2. Figures displaying the molecules have been generated using a combination of CCP4mg (52), Pymol (Schrödinger) and UCSF ChimeraX (53).

Results

Here, we aimed to functionally and structurally characterize the transcription-related activities of the SFTSV L protein as a model phenuivirus. To this end, we established an *in vitro* cap-snatching reaction in which we can visualize capped RNA cleavage and subsequent incorporation of the capped primer into transcription products. We also report three high-resolution structures of the SFTSV L protein representing snapshots of the viral genome transcription process by single-particle cryo-EM providing a structural basis for phenuivirus cap-snatching. An overview of the structures including their key features is provided in Table 1.

Establishing an *in vitro* cap-snatching reaction

To explore cap-snatching *in vitro*, we incubated the wild-type SFTSV L with three RNA species: 5′ (1–20) and 3′-6A (1–26) RNA, which correspond to the SFTSV genome termini (large segment), and a 32 nucleotides (nt) primer modified with the addition of either a diphosphate (Primer B-PP) or cap^0 (Primer B-CAP) at the 5′ end making for a total length of 32–33 nts. The rationale behind the length of this primer stems from sequencing data showing that phenuiviruses typically snatch primers in the range of 12–14 nts (22). Thus, we wanted to ensure the primer was sufficiently long so as to engage both the CBD and ENDO. The reaction mix was incubated at 30°C between 1 and 60 min with samples taken at regular time inter-

Table 1. Overview of cryo-EM structures

Name	Res (Å)	RNA	PDB Code	EMDB Code	Comment
TRANSCRIPTION-PRIMING	3.35	L 5′ (1–20) L 3′-6A (1–26) Primer C-CAP (1–17)	8R6W	EMD-18967	The L protein N- and C-terminal domains are largely rearranged enabling the CBD to feed the bound capped-RNA into the RdRp core. The L protein is also bound to the 5′ and 3′ RNAs, which form a distal duplex structure, with the 3′ RNA feeding into the RdRp core. The tail-end of the capped RNA is shown to base-pair with the 3′ RNAs. Although the 5′ and 3′ ends of the capped primer can be fit with some confidence, it is not possible to fit the entire length of the primer into the map.
TRANSCRIPTION-EARLY-ELONGATION	3.40	L 5′ (1–20) L 3′-mid AAA (1–20) Primer C-CAP (1–17)	8R7Y	EMD-18969	The L protein N- and C-terminal domains remain in the priming state. The L protein is bound to the 5′ and 3′ RNAs, which form a distal duplex structure and the 3′ RNA feeds into the RdRp core. However, the 3′ RNA between the distal duplex and the entrance to the RdRp core appears under strain/tension. There is a stalling UpNHpp at the +1 position indicating that elongation has started but not progressed far.
TRANSCRIPTION-PRIMING (*in vitro*)	2.98	L 5′ (1–20) L 3′-6A (1–26) Primer C-CAP (1–17)	8R6U	EMD-18963	The L protein N- and C-terminal domains are found in their 'apo' positions with the ENDO now sitting across the floor of the RdRp core. The L protein is bound to the 5′ and 3′ RNAs, which form a distal duplex structure, with the 3′ RNA feeding into the RdRp core. There are nts shown base-pairing with the 3′ RNA in the RdRp core, however, given NTPs were missing for this reaction, these nts are likely primer. The capping reaction is not 100% effective and so we have a mixture of triphosphorylated primer and capped primer in the reaction mix. The primer base-pairing with the 3′ RNA in the RdRp core here is likely therefore uncapped primer, hence, explaining why the CBD is not involved in comparison with the TRANSCRIPTION-PRIMING structure.

An overview of the cryo-EM structures is provided with the reported resolution (Å), any RNA ligands present, PDB and EMDB accession codes, as well as supporting comments highlighting the key features of each structure.

vals. In the presence of an uncapped diphosphorylated primer, the L protein produces a major product at around 54–56 nts (Figure 1, left panel). Here, the primer is at a 5-fold excess to the 5′ and 3′ RNAs and it seems that *de novo* unprimed synthesis is not a preferred mode of activity, based on the lack of a major product at the expected size of 26 nts. We propose that the major product at 54–56 nts corresponds to the L protein using the full-length primer to initiate RNA synthesis. This can be achieved *via* the 3′ end of the primer, which consists exclusively of AC repeats ($n = 10$), base-pairing with the terminal 3′-UGUG…-5′ of the 3′ RNA. This product band is noticeably smeared, which would indicate that the primer and template are base-pairing in a variable fashion rather than consistently (Figure 1, left panel). For example, the terminal AC repeat on the primer could base-pair with the terminal UG of the 3′ RNA or, alternatively, the terminal ACAC on the primer could base-pair with the terminal UGUG of the 3′ RNA. This would then lead to similarly-sized products that vary by 2 nts. Formation of this major 54–56 nts product is clearly detectable from the 5 minute timepoint onwards and then gradually decreases in intensity until the 1 h timepoint (Figure 1, left panel), when the band is very faint. This is accompanied by a clear shift in the band profile at the lower end of the gel, where the intensity of the smaller '*product*' bands increases with time (Figure 1, left panel). These bands most likely correspond to fragments of RNA that have been degraded over time by the SFTSV L protein endonuclease.

In the presence of the 32-mer capped RNA, the major product appears to be at 39 nts rather than 54–56 nts (Figure 1, left panel). We propose this corresponds to a cleaved-capped primer-incorporated product wherein the primer was generated by cap-snatching: the capped RNA is bound initially by the CBD, then cleaved around nt 15 by the ENDO and finally inserted into the RdRp active site. Here, the primer base-pairs with the template enabling RNA synthesis initiation. This primer length would fit with the reported 12–14 nts of non-viral sequences at the 5′ ends of other phenuivirus transcripts (Figure 1, left panel) (22). The capped RNA fragment produced would end at the 3′ terminus with an ACA which could then base-pair with the terminal UGU of the 3′ template RNA.

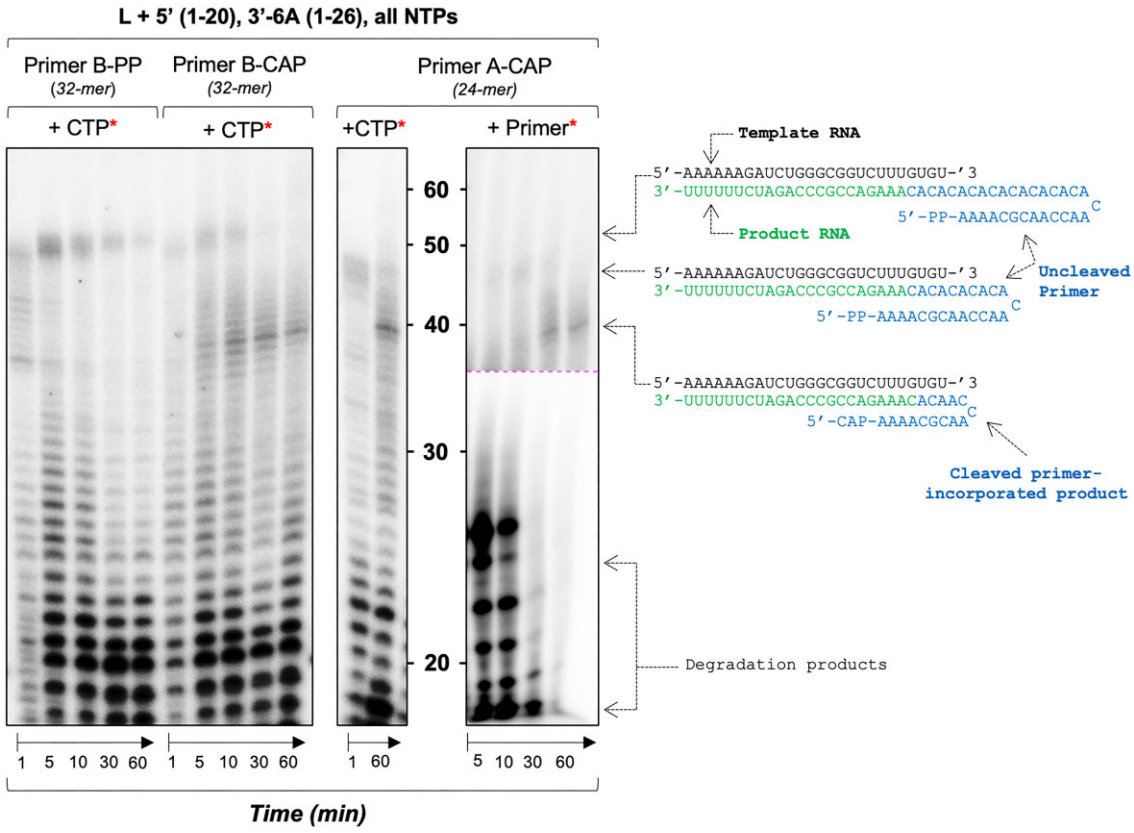

Figure 1. Establishing an *in vitro* cap-snatching reaction. (Left panel) The impact of primer capping in the presence of the wild-type SFTSV L protein was tested *in vitro*. The reactions were carried out with the L 5′ (1–20), L 3′-6A (1–26), and a 32 nt primer that was either diphosphorylated at the 5′ end or capped through the addition of an m^7GTP cap under standard polymerase assay conditions (see Materials and Methods). (Central panel) The impact of primer length was then tested *in vitro*. The reactions were carried out with the wild-type L protein, which was incubated with the L 5′ (1–20), L 3′-6A (1–26) and a 24 nt primer that was capped through the addition of an m^7GTP cap at the 5′ end as per our standard polymerase assay conditions (see Materials and Methods). (Right panel) To confirm the obtained 39 nt product was in fact a primer-incorporated product, the cap-snatching assay was repeated using a radiolabelled capped primer. The reactions were carried out with the wild-type L protein, which was incubated with the L 5′ (1–20), L 3′-6A (1–26) and a 24 nt primer that was capped through the addition of a radiolabelled m^7GTP cap at the 5′ end (see Materials and Methods). For all reactions, samples were taken at regular time intervals between 1 and 60 min. Products were separated by denaturing gel electrophoresis and visualized by autoradiography.

In a similar fashion to the uncapped primer reaction, we see noticeable amounts of cleaved capped-primer incorporated product from the 5–10 min timepoint with endonuclease-mediated degradation then apparent as the reaction proceeds (Figure 1, left panel). Curiously, there remains a small amount of full-length product in which the primer apparently has not been cleaved (Figure 1, left panel). We think the reason for this is that the capping reaction is not 100% efficient, therefore we expect that in our capped RNA preparation, a small amount of uncapped disphosphorylated primer remained. We suspect that this leftover uncapped disphosphorylated primer is the reason we still see some product resulting from priming by a full-length (uncleaved) RNA primer.

We hypothesized that the size of the snatched fragment (here this is 15 nt) was dictated at least in part by the physical distance between the cap-binding site of the CBD and the active site of the ENDO. In theory, it should not matter how long the capped primer is, provided it meets the minimum structural requirements, which are reported to be in the range of 12–18 nts (20). Thus, we should see the same cleaved-capped primer-incorporated product. To test this hypothesis, we repeated our *in vitro* cap-snatching assay with a shorter capped primer that was 24 nts long (Primer A-CAP, Supplementary Table S1) instead of 32 nts and detected an identical cleaved-capped primer-incorporated product for which the primer must have been cleaved to the same extent (Figure 1, central panel). Out of an abundance of caution, and to conclusively demonstrate that the product at 39 nts was in fact primer-incorporated, we capped and labelled Primer A-PP using radioactive GTP and, as a result, produced a radiolabelled Primer A-CAP. When incorporated into our cap-snatching assay, on any readout, the only bands visible would be those that include the radiolabelled-capped RNA. Repeating the cap-snatching assay with this radiolabelled-capped RNA resulted in a much cleaner gel that clearly shows that the product at 39 nts includes radiolabelled-capped RNA (Figure 1, right panel). We could observe that, with time, the intensity of the bands for the primer alone, which migrated at the expected size on the gel, was slowly degraded 2–4 nts at a time. To conclude, here, we demonstrate the full process of cap-dependent transcription initiation by a bunyavirus L protein *in vitro* starting with primer generation by cap-binding and ENDO activities, followed by cap-primed RNA synthesis by the RdRp.

The SFTSV L protein transcription priming structure

Next, we sought to visualize by single-particle electron cryo-microscopy (cryo-EM) the conformational and structural changes associated with viral genome transcription by cap-snatching for the SFTSV L protein. To first visualise the SFTSV L protein in a transcription-specific priming state, we incubated the L protein with 5′ and 3′ RNA and a capped RNA primer (17 nts including the 5′ cap^0 structure), which was in 6-fold molar excess to the 5′ and 3′ RNA species. To ensure that the L protein could not proceed to elongation, this reaction was set up in the absence of NTPs. This ultimately yielded a 3.35 Å resolution structure that we refer to as TRANSCRIPTION-PRIMING. Here, the 5′ and 3′ RNAs form the expected distal duplex with the 3′ RNA feeding into the L protein core (Figure 2A). However, we observe the domains at the N and C termini of the L protein have adopted a novel arrangement (Figure 2A). Whereas, in our published replication-mode LATE-ELONGATION structure (19) the CBD is found in a peripheral location proximal to the ENDO, here the CBD is found at the base of the L protein. Bound to the CBD we found capped RNA, which as a result of the rearrangement of the ENDO and CBD is now oriented such that it feeds directly into the L protein core: 4 nts of the capped RNA 3′ end base-pair with the 3′ RNA template in the RdRp active site (Figure 2A; Supplementary Figure S3).

The ENDO domain has rotated by around 170° away from the base of the RdRp core in respect to its position in the *apo* conformation of L (18) (Figure 2B). Importantly, the movement of the ENDO domain creates sufficient space into which the CBD can then rotate by approximately 90° (Figure 2B). It is noteworthy that this position of the ENDO in the TRANSCRIPTION-PRIMING structure is significantly different to the '*raised conformation*' we reported in our genome replication-related EARLY-ELONGATION-ENDO structure (19). In total, we have now visualized the ENDO domain in three different conformations (Supplementary Figure S4). Interestingly, the endonuclease linker, which connects the endonuclease domain to the RdRp core does not appear to change significantly either its position or secondary structure (Supplementary Figure S4). The key appears to be the hinge region (residues 206–218), which connects the ENDO domain to the linker. This hinge region is largely unstructured in our previously published SFTSV L protein structures, with the exception of the EARLY-ELONGATION-ENDO structure (19). It appears that this short stretch of amino acids imparts significant flexibility to the SFTSV L ENDO domain.

The outcome of these multi-domain conformational changes is that the putative cap-binding site is no longer oriented towards the solvent, as observed in our published LATE-ELONGATION structure (19), but instead oriented towards the RdRp core. In this conformation, bound capped RNA can proceed directly into the RdRp core to base-pair with 3′ RNA. Furthermore, the arginine finger blocking motif (composed of residues I1839–V1844), that we and others found occluding access to the cap-binding site (19), has retracted with the blocking R1843 sidechain now sitting orthogonally to the cap-binding pocket (Figure 2C). Inspection of the map around the putative cap-binding site shows capped RNA bound with the guanosine moiety sandwiched between two aromatic sidechains: F1703 and Y1719 (Supplementary Figure S5). This mode of binding agrees with that described in the X-ray crystal structure of the SFTSV CBD in complex with the cap-analog m^{7}GTP (18).

There are further stabilizing interactions between the cap structure and nearby residues. These include Q1707, which interacts with the cap guanosine, as well as K1668 and L1772, which coordinate the cap ribose via the O3′ and O2′ hydroxyls, respectively. There are extensive interactions between the cap^0 triphosphate linker and residues from the C terminus of the L protein, including the sidechains of Y1719, N1834, N1846 and S1849. These sidechains interact with one or more phosphate oxygens and in doing so support cap-binding (Figure 2D). It is worth noting, that the interactions with the triphosphate moiety seen here differ slightly from the published crystal structure, however, that is perhaps to be expected given that we are looking at the full L protein in the structures published here (18). Although the cap guanosine is bound perpendicular to the L protein core, the cap triphosphate linker points towards the RdRp active site. This is principally a result of amino acids from the C terminus, inclusive of M1845 – P1852 and T1838–D1831, which direct the triphosphate linker and therefore the remaining nts attached to the cap structure towards the RdRp active site (Figure 2D). The quality of the map allows to confidently fit the first 3 nts of the capped RNA, and this corresponds to 5′-cap^0-AAA-3′. These 3 nts are supported by long range electrostatic interactions which coordinate RNA ribose and phosphate groups (Supplementary Figure S6). There appear to be no specific sidechain-capped RNA base interactions indicating that the SFTSV L protein has little sequence specificity for the RNA snatched.

Similar to our published EARLY-ELONGATION structure (19), in the TRANSCRIPTION-PRIMING structure, the 5′ RNA binds in a hook-like conformation in a positively-charged cleft formed by residues from the vRNA binding lobe (vRBL), fingers domain, and PA-C like core lobe. The 5′ and 3′ RNA then form a duplex stabilized by interactions between nts in the distal ends of the 5′/3′ RNAs, which positions the 3′ RNA template in the RdRp active site ready for initiation. We can fit an unbroken chain of 3′ RNA nts from the distal duplex to the RdRp active site, allowing us to determine that the template is 4 nts into the active site with G4 at the +1 position (Supplementary Figure S3). Similar to that seen in our EARLY-ELONGATION structure (19), the 3′ RNA between the distal duplex and the RdRp active site is relatively condensed and appears to be anchored in place by the G10 base, which sits in a pocket delineated by W1342–K1347 and L1399–S1400 (Supplementary Figure S7). Further inspection of the map in the RdRp core itself, led us to discover a 4 nts long RNA in the product position base-pairing with the 3′ RNA template (Supplementary Figure S3). Given that the L protein was incubated without any NTPs in this condition, it is not possible for this RNA to be an L protein synthesized product. We therefore propose these 4 nts correspond to the tail-end of the capped RNA, whose cap is bound to the CBD sitting at the base of the RdRp core.

The primer used in these experiments is designed to have a 4-bp overlap with the 3′ RNA template. In this schema, C1 of the primer base-pairs with G4 of the template RNA while A2 of the primer base-pairs with U3 of the template RNA (Supplementary Figure S3). This repeats with C3 and A4 of the primer which base-pair with G2 and U1 of the template RNA, respectively. The quality of the map in the TRANSCRIPTION-PRIMING structure is sufficient to

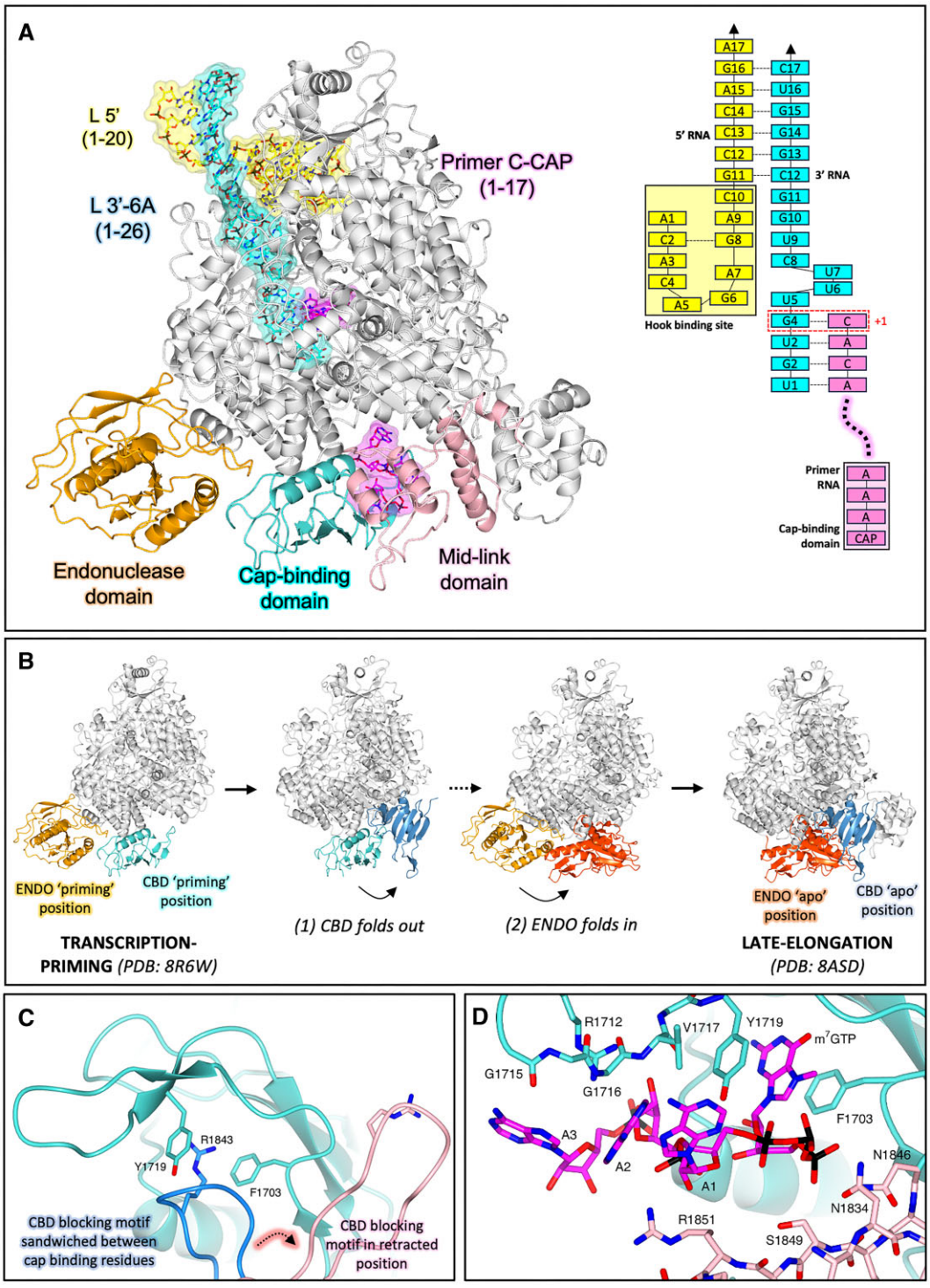

Figure 2. The SFTSV L protein transcription priming structure. (**A**) The SFTSV L protein (TRANSCRIPTION-PRIMING) is shown with key L protein domains coloured according to the following colour scheme: endonuclease (orange), cap-binding domain (cyan), and mid-link domain (light pink). RNAs are shown as sticks with surface overlaid (30% transparency) and coloured either yellow (5′ RNA), cyan (3′ RNA), or magenta (primer RNA). In addition, the RNAs present in each structure are shown schematically and labelled. (**B**) The conformational changes undergone by the L protein as it moves from transcription-priming to late-elongation are shown. L protein domains are coloured as in A. For clarity, RNA is not shown. (**C**) The position of the cap-binding domain (shown in cyan) blocking motif (composed of the Q1840 and R1843 sidechains) is shown sandwiched between the putative cap-binding residues (F1703 and Y1719) in the published LATE-ELONGATION structure (PDB:8asd, coloured dark blue) and in a retracted position in the TRANSCRIPTION-PRIMING structure published here (coloured light pink). (**D**) The cap-binding domain is shown with bound capped RNA. The cap-binding domain is coloured cyan, whereas the neighbouring mid-link domain is shown in light pink. The bound capped RNA is shown as sticks. Sidechains of key interacting amino acids, coloured according to the protein domain, are shown as sticks and labelled accordingly.

fit the C1, A2, C3 and A4 of the primer with confidence (Supplementary Figure S3). C1 is supported by several long interactions which coordinate the C1 ribose O2′ (R920, Q1080, G1081) and O3′ hydroxyl groups (H1084). While A2 is coordinated by the S1125 sidechain, C3 is supported by interactions from the N1182 and R1197 sidechains. A4 is coordinated principally by the Q1204 and Q1224 sidechains. After A4, the map degrades to such an extent that fitting any further primer nts becomes speculative. It is noteworthy that while we can fit the 5′ and 3′ ends of the capped primer, we are missing effectively half of the primer nts from the map. This is likely because of the general lack of interacting sidechains to stabilize those nts as they travel from the CBD to the RdRp active site.

The transition from cap-snatching to early-elongation

We next sought to capture the SFTSV L protein immediately after cap-snatching as it begins the process of primer elongation. For this, we incubated the L protein with nts 1–20 of the 5′ RNA, a modified 3′ RNA template (3′-midAAA) in addition to a 16 nt primer with a cap^0 structure together with ATP, GTP, CTP, and a non-hydrolysable analog of UTP, specifically: uridine-5′-[(α,β)-imido]triphosphate (UpNHpp). The modification of the template, in which nts 6–8 are replaced with A's, allowed us to stall the L protein *via* incorporation of UpNHpp 2 nts downstream of the primer, which was designed to base-pair with nts 1–4 of the template RNA. This approach led to a single high-resolution structure, which we refer to as the TRANSCRIPTION-EARLY-ELONGATION (3.40 Å) structure (Figure 3A).

We note that the ENDO has moved by several angstroms away from the base of the L protein and the C terminus, which includes the Lariat domain, has rotated towards the L protein core (Supplementary Figure S8). These movements correlate with the shunting of the capped primer (still bound by the CBD) by 2 nts as a result of the short elongation reaction while the 3′-5′ distal duplex region still stays intact. Furthermore, similar to the TRANSCRIPTION-PRIMING structure, we can fit an unbroken chain of 3′ RNA nts feeding directly from the distal duplex into the RdRp active site. However, herein lies a key difference. In the TRANSCRIPTION-PRIMING structure, at the splitting of the distal duplex, the 3′ RNA inverts at G10 and is then shown to '*bunch up*' immediately before entering the RdRp core. Instead, the 3′ RNA in the TRANSCRIPTION-EARLY-ELONGATION structure is shown to feed directly in to the RdRp core without inflection or bunching (Supplementary Figure S8). This is something that we have seen previously, for example, in our replication-mode EARLY-ELONGATION structure (19). However, in that structure, the 3′ RNA only proceeds 4 nts into the RdRp core with G4 shown to rest at the +1 position. In the TRANSCRIPTION-EARLY-ELONGATION structure published here, the 3′ RNA proceeds 6 nts into the RdRp core and A6 is shown at the + 1 position. Importantly, in both structures, the distal duplex remains intact. Thus, we can surmise that the 3′ RNA in the TRANSCRIPTION-EARLY-ELONGATION structure is likely under an element of tension by virtue of proceeding further into the RdRp core while remaining anchored in place by the distal duplex.

We also note that the inner L protein core has started to expand, presumably to accommodate the growing product-template duplex, which we find to be only partly defined in the map. In the RdRp core, the quality of the map is sufficient to fit the terminal nucleotides 3–6 of the 3′ template RNA (5′-A6-U5-G4-U3-3′) with A6 sitting at the +1 position (Figure 3B). Opposite A6, we can fit the stalling UpNHpp, the tail of which is shown to support the coordination of a single Mg^{2+} ion alongside A986 and D1126. Adjacent to the UpNHpp, we can fit 3 nts of the '*product RNA*', which in this structure is 5′-ACA-3′. The primer used in this reaction was designed to base-pair with nts 1–4 of the 3′ RNA. We conclude that the 3′-terminal A and C in this short product correspond to the last 2 nts in the capped primer, with the second A representing the first nt added by the L protein after priming. The L protein had successfully primed RNA synthesis using the capped-RNA provided and then proceeded to elongation at position 5 of the 3′ RNA. Stalling occurred at position 6 of the 3′ RNA template, which corresponds to the first A in this specifically designed template sequence. In comparison to the TRANSCRIPTION-PRIMING structure, the 3′ RNA template has been pulled forward by two nts and, as a result, the preceding nts feeding up to the distal duplex are now under tension. This tension, however, has not yet caused the distal duplex to dissolve.

It is noteworthy, that we do not resolve the first two 3′ RNA nts or the two nts from the capped-RNA, to which they are base-paired in the map. We suggest this is principally due to the openness of the inner L protein core at this stage in the elongation process. There are very limited potential protein sidechains that could stabilize a growing product-template duplex and we clearly do not have the same number of RNA-RNA interactions that likely contribute to the stabilization of the 10-bp product-template duplex observed in our previously published replication-focussed LATE-ELONGATION structure (19). The growing product-template strands head towards the base of the L protein core, which remains buttressed by the CBD bound to the capped RNA. This is reasonably clear in our final polished cryo-EM map, where at lower contours the density for the product RNA connects to the density feeding from the bound cap-RNA fragment. We are confident therefore, that what we are seeing in this structure is the capped RNA bound simultaneously to the CBD, which remains in the priming position, and the 3′ RNA in the RdRp active site. We have chosen, however, not to fit the complete primer into the EM map, principally because of the poor nature of the map outside of the immediate primer termini. It is clear that the middle part of the primer retains significant flexibility adopting a range of orientations and we therefore cannot fit it with confidence.

In the TRANSCRIPTION-PRIMING and TRANSCRIPTION-EARLY-ELONGATION structures, we can now fit a significant portion of the extreme C terminus of the L protein, which thus far has been missing or poorly defined in other reported structural data. As a result, we can confidently fit the overwhelming majority of the L protein residues with only 4.3% of the entire L protein (90 amino acid residues) missing. There are further conformational changes to the L protein as we move from priming by cap-snatching to early-elongation of transcription, the most apparent being with respect to the CBD and Lariat domain (Supplementary Figure S8). Firstly, progression of the elongation reaction appears to have a shunting effect on the ENDO and CBD, which, when compared to the TRANSCRIPTION-PRIMING structure, are shown to recede slightly from their

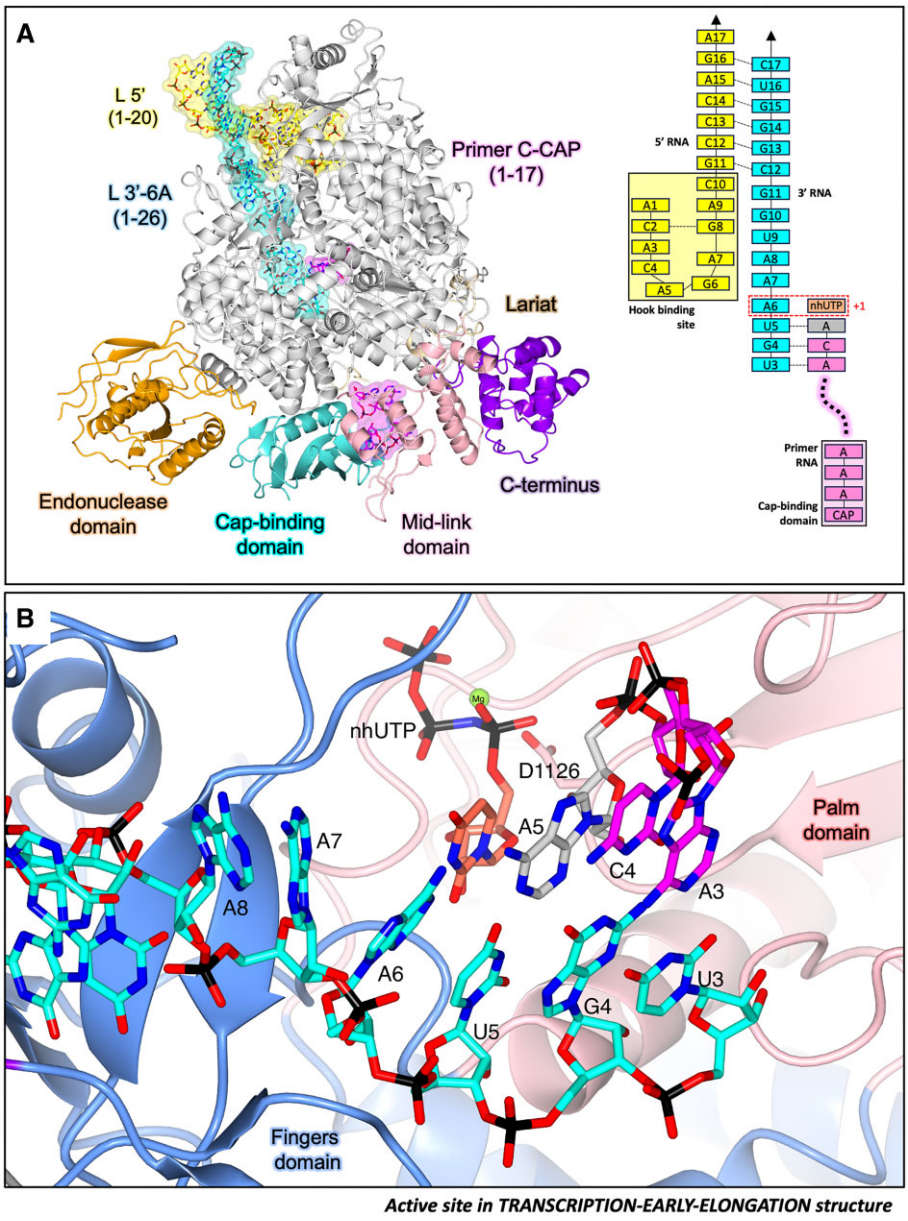

Figure 3. The transition from cap-snatching to early-elongation. (**A**) The SFTSV L (TRANSCRIPTION-EARLY-ELONGATION) is shown with key L protein domains coloured according to the following colour scheme: endonuclease (orange), cap-binding domain (cyan), and mid-link domain (light pink). RNAs are shown as sticks with surface overlaid (30% transparency) and coloured either yellow (5′ RNA), cyan (3′ RNA), or magenta (primer RNA). In addition, the RNAs present in each structure are shown schematically and labelled. (**B**) The active site in the TRANSCRIPTION-EARLY-ELONGATION structure is shown. Residues from the L protein are labelled and coloured according to the assigned domain (blue for fingers domain, and coral for the palm domain). RNAs are shown as sticks and coloured as in A.

priming positions. Secondly, the C-terminal Lariat domain is shown to rotate and move towards the L protein core, presumably in response to the movement of the CBD. These domain movements are relatively fine and we think this can be explained by examining the inner L protein core. The internal L protein cavity is a relatively open space at this point in the elongation process. It is therefore entirely conceivable that the procession of the product-template strands by 2 nts (by comparison to the TRANSCRIPTION-PRIMING structure) can be largely '*absorbed*' by the openness of the L protein core. That being said, there is clearly a finite amount of space available. We expect the precession of the product-template strands to eventually be such that the CBD will need to move in a more significant manner, ultimately returning to its '*apo*' position (19).

Mutational analysis of capped RNA-interacting residues

The TRANSCRIPTION-PRIMING and TRANSCRIPTION-EARLY-ELONGATION structures have provided us with the first opportunity to identify amino acid residues involved in binding capped RNA in the cell. The capped RNA in the TRANSCRIPTION-PRIMING and TRANSCRIPTION-EARLY-ELONGATION structures appear coordinated by a mixture of sidechain-RNA phosphate and sidechain-RNA

base interactions. The key residues of the CBD interacting with the m^7GTP have already been tested previously (24). However, sidechains interacting with nts downstream of the m^7GTP cap have overall not been tested. To investigate the importance of the additionally interacting sidechains, we mutated 19 different amino acids of the L protein and tested for genome replication and transcription activity in a cell-based viral mini-replicon system.

As SFTSV is closely related to RVFV, we superposed the 3D models (Supplementary Figure S9) and mapped the identified SFTSV residues onto the RVFV L protein. We then mutated the corresponding side chains in RVFV L and tested these mutants in our established RVFV mini-replicon system (Figure 4, Supplementary Figure S10), an approach also taken in Williams and Thorkelsson et al. (2023) (19). Of the 19 mutants tested, 8 showed wild type-like activity (*i.e.*, Ren-Luc activity, >50%), including: V965G (SFTSV: N959), D1497A (SFTSV: Q1504), S1719A (SFTSV: T1709), V1726G (SFTSV: V1717), R1841A (SFTSV: R1829), S1861A (SFTSV: S1849), T1863A (SFTSV: R1851), and S1865A (SFTSV: R1853). Four mutants including S1231A (SFTSV: Q1224), E1565A (SFTSV: R1582), K1680A (SFTSV: K1668) and N1846A (SFTSV: N1834) demonstrated reduced L protein activity (*i.e.*, Ren-Luc activity, 8–49%) (Supplementary Table S3). We also found mutations to a small number of sidechains that led to an inactive L protein phenotype (*i.e.*, Ren-Luc activity, 0–7%), including R1200A (SFTSV: R1193), W1205G (SFTSV: W1198), R1501A (SFTSV: R1499), T1563A (SFTSV: S1580) and H1858A (SFTSV: N1846) (Supplementary Table S3).

Of these inactivating mutations, the majority of the residues are located in the RdRp core and could possibly be involved in stabilizing the capped primer as it base-pairs with the 3′ RNA. As these residues line the walls of the RdRp core itself, it is also possible that altering the nature of the charged surface then impedes progression of the product-template duplex. Indeed, in previous studies, we have mutated adjacent residues thought to interact directly with the growing product-template duplex (*e.g.*, SFTSV residues H1084 and F1085) and found that they also led to an inactive L protein (19). The only other mutant leading to an inactive L protein was H1858A (SFTSV: N1846), which coordinates the m^7GTP α-phosphate. It is not entirely clear why mutating this residue has such a global effect but it is possible that it has a destabilizing effect.

Other mutations, like those to V1726, R1841, S1861, T1863 and N1846 are particularly interesting because it seems that the ∼50% reduction in the mRNA signal on the Northern blot is met with a 2-fold increase in the signal for antigenomic RNA (Supplementary Figure S10). This would suggest that disruption to these sites may inhibit conformational changes associated with transcription activity while leaving the L protein still capable of catalysing genome replication. This aligns with our structural insights into genome replication by the SFTSV L protein which does not appear to involve structural rearrangements to the C-terminal region (39). We might also speculate a regulatory role for residues in the C-terminal domain in driving the balance between viral RNA genome replication and transcription. However, none of the mutants completely abolished the L proteins ability to undergo genome replication or transcription suggesting that the sidechains tested are not individually essential and do not critically impact viral transcription, genome replication or expressability of the L protein.

We also know that under certain conditions the SFTSV cap-binding site is blocked by an arginine finger motif composed of the Q1840 and R1843 sidechains (Figure 2C). In our TRANSCRIPTION-PRIMING and TRANSCRIPTION-EARLY-ELONGATION structures, this motif is displaced by our capped primer but we nevertheless wanted to evaluate the importance of these two sidechains in our RVFV mini-replicon system (Figure 4). While the Q1855A (SFTSV: R1843) mutant showed a close to wild type-like phenotype, the H1852A (SFTSV: Q1840) mutant showed a largely reduced L protein activity (Supplementary Figure S10) (Supplementary Table S3). There was no selective effect on viral transcription detectable in the Northern blot. Thus, we concluded that the absence of this blocking motif may not directly lead to enhanced transcriptional activity. It is plausible, that the interaction of this blocker motif with the cap-binding site may primarily be a way for the L protein to stabilize a relatively flexible surface loop (including the blocker motif) rather than autoinhibiting the CBDs cap-binding capabilities.

Structural insights into cap-independent primer elongation observed *in vitro*

In cells, we know that bunyaviruses, including SFTSV, must cap-snatch in order to produce their viral proteins. Translation is normally a cap-dependent process. It is curious therefore that, *in vitro*, we have also seen uncapped priming of RNA synthesis by SFTSV L protein (18,19). This is a phenomenon reported multiple times for different bunyaviruses. Indeed, for some bunyaviral L proteins it has been difficult to demonstrate cap-dependent primer elongation at all, such as LASV (33). However, it has not been clear how these different bunyaviral L proteins incorporate uncapped RNA primers into their growing strands. The TRANSCRIPTION-PRIMING (*in vitro*) structure (2.98 Å) we include here, provides the first structural insights into how this might happen in practice (Figure 5).

Here, the L protein adopts an overall similar conformation to that seen in our previously published EARLY-ELONGATION structure (19), a snapshot of the genome replication process. In the TRANSCRIPTION-PRIMING (*in vitro*) structure, the ENDO has returned to its '*apo*' position (19), now sitting across the base of the L protein core. For this structure, we specifically wanted to visualise transcription priming without allowing elongation to begin and so this reaction was incubated in the absence of NTPs. The 5′ RNA binds in a hook-like motif between the vRNA binding lobe (vRBL), fingers domain, and the PA-C like core lobe. The distal ends of the 5′ and 3′ RNAs form a distal duplex and the quality of the map allows us to fit the 3′ RNA nts feeding from the distal duplex to the RdRp active site. We could determine therefore that, in a similar fashion to that seen in our EARLY-ELONGATION and EARLY-ELONGATION-ENDO structures (19), the 3′ RNA sits 4 nts into the L protein active site with G4 at the + 1 position. There is density present for nts that would base-pair with the 3′ RNA in the L protein core. Given that no NTPs were provided for this reaction and that there is no incoming nucleotide at the + 1 position, we propose this corresponds to nts from the RNA primer that have base-paired with the template RNA. We propose the TRANSCRIPTION-PRIMING (*in vitro*) structure corresponds to something fairly routinely observed *in vitro*, that is cap-independent primer elongation. This would explain why

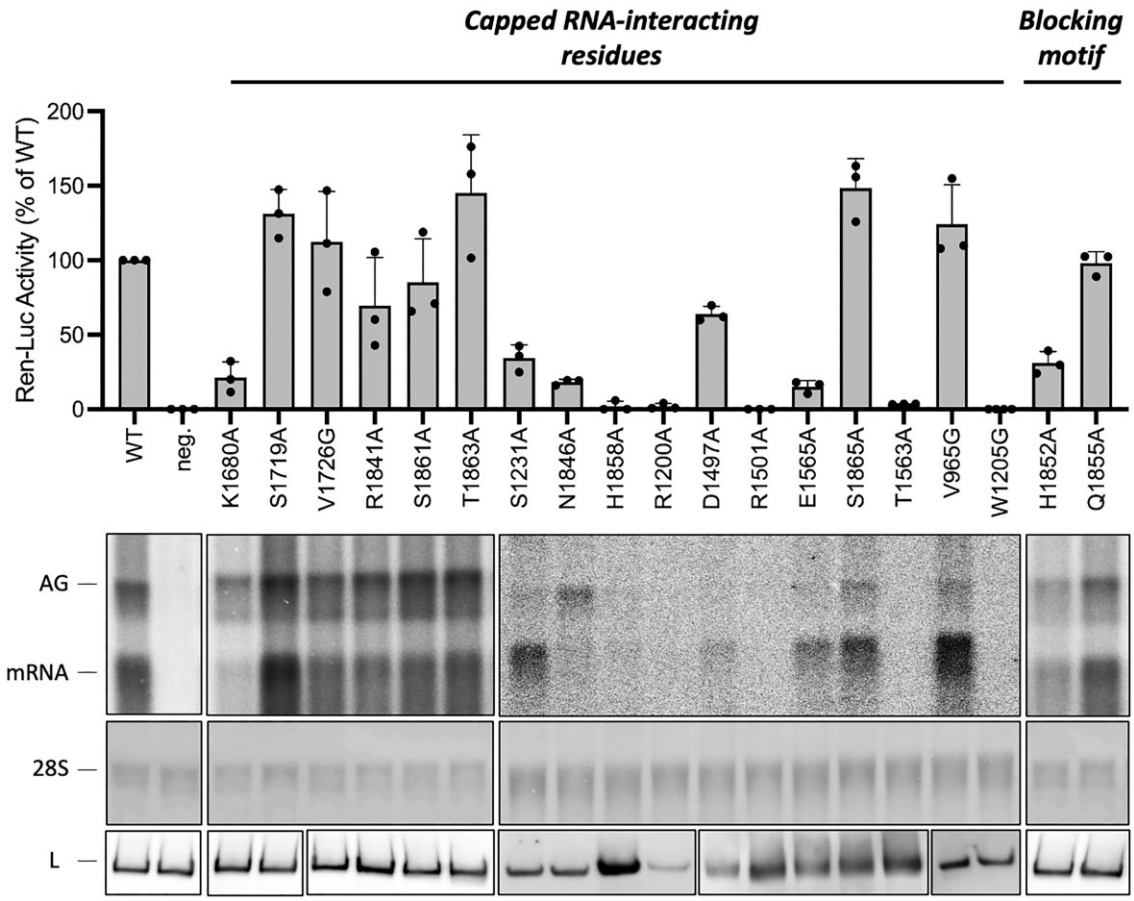

Figure 4. Mutational analysis of capped RNA-interacting residues. RVFV mini-replicon data for L protein with mutations to capped RNA-interacting residues presenting luciferase reporter activity (in standardized relative light units relative to the wild-type L protein (WT)). Data were presented as mean values ± SD of three biological replicates ($n = 3$). All biological replicates are shown as black dots (top panel). Middle panels present Northern blotting results with signals for antigenomic viral RNA (AG, equal to cRNA), viral mRNA (mRNA) and 28 S ribosomal RNA (28 S) as a loading control, and the bottom panel shows Western blot detection of FLAG-tagged L proteins (L) to demonstrate general expressability of the mutants. Fast green staining of the membranes is included in the Supplementary data. The Western blots have not been used for quantification.

the CBD and ENDO domains are in their '*apo*' positions. The capping reaction with which we add a cap^0 structure is not 100% efficient and therefore uncapped triphosphorylated primer is expected to remain in the reaction. We also know from our TRANSCRIPTION-EARLY-ELONGATION structure that the CBD and ENDO conformations associated with transcription priming are retained in the earliest stages of primer elongation. Finally, the lack of NTPs in this reaction would not even allow elongation to occur. We think it likely then that the primer/product RNA base-pairing with the 3′ RNA in the TRANSCRIPTION-PRIMING (*in vitro*) structure is in fact carryover uncapped triphosphorylated primer RNA. This would explain why the CBD does not appear to be involved in the same way that we see in the TRANSCRIPTION-PRIMING structure. Thus, what we assume to have here, is structural evidence for cap-independent priming, which we also observe in our *in vitro* assays.

In our TRANSCRIPTION-PRIMING structure, we demonstrate that capped RNA fragments are incorporated into RNA synthesis products as a result of significant domain reorganization, principally relating to the CBD and ENDO domains. However, that does not appear to be the case here in the TRANSCRIPTION-PRIMING (*in vitro*) structure. Instead, the reorganization of the L protein is far more nuanced and reminiscent of our EARLY-ELONGATION structure related to genome replication (19). Specifically, there is a rotation of the ENDO domain towards the L protein core, which provides space for part of the thumb ring domain (~L1509–K1577) to rotate away from the L protein core, moving into the space vacated by the ENDO domain (Supplementary Figure S11). These movements lead to an opening up of the putative product exit channel and we propose that it is *via* this channel that the non-capped primer RNA enters the L protein core, the terminal nts of which ultimately then base-pair with the 3′ template RNA (Supplementary Figure S11).

Discussion

Bunyaviruses need to snatch capped RNA primers for transcription priming in order to access the cellular translation machinery. This cap-snatching process is handled in large part by the viral L protein. Understanding how the L protein enables cap-snatching and therefore viral transcription is important not only to increase our fundamental understanding of bunyaviruses but also for the rational design of therapeutic interventions. Here, we establish an *in vitro* cap-snatching assay and report several high-resolution cryo-EM structures of

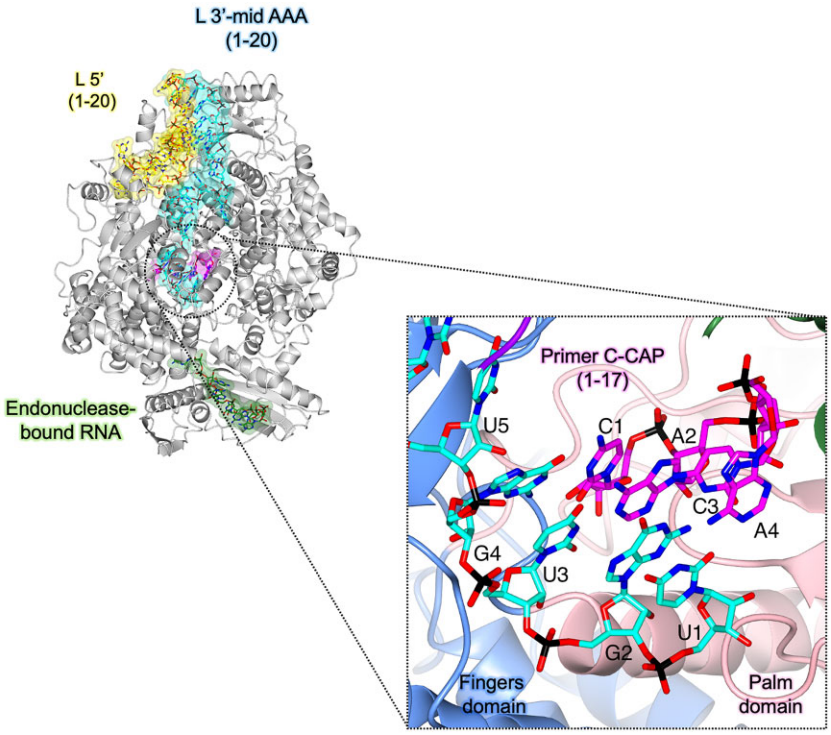

Figure 5. Structural insights into cap-independent primer elongation observed *in vitro*. The SFTSV L (TRANSCRIPTION-EARLY-ELONGATION (*in vitro*)) is shown with bound RNAs shown as sticks with surface overlaid (30% transparency) and coloured either yellow (5′ RNA), cyan (3′ RNA), magenta (primer RNA), and sea green (endonuclease-bound RNA). A zoomed-in view of the active site in the TRANSCRIPTION-EARLY-ELONGATION (*in vitro*) structure is also shown with residues from the SFTSV L protein labelled and coloured according to the assigned domain (blue for fingers domain, and coral for the palm domain).

the SFTSV L protein in the early-stages of viral transcription (Figure 6).

Comparison of our TRANSCRIPTION-PRIMING structure to our previously published SFTSV L protein structures mimicking viral genome replication is particularly insightful (18,19). It demonstrates that, after binding to capped RNA, the N-terminal ENDO and C-terminal CBD of the SFTSV L protein undergo a significant conformational change (Figure 2). In the genome replication-associated LATE-ELONGATION structure, the CBD is oriented such that bound capped RNA would be directed away from the RdRp (19). We suspect that the positioning of the CBD in this LATE-ELONGATION structure likely represents a fishing conformation by which the L protein can capture nearby host cellular mRNAs. The major domain reorganization in our TRANSCRIPTION-PRIMING structure ultimately repositions the capped RNA-bound CBD such that it then sits across the floor of the L protein (Figure 6). This enables the CBD-bound capped RNA to feed directly into the RdRp core and base-pair with the 3′ RNA template. Addition of NTPs spiked with a stalling UpNHpp that stalls 2 nts downstream of the incorporated primer shows that this transcription priming state is retained in our TRANSCRIPTION-EARLY-ELONGATION structure suggesting that perhaps it is the progression of the growing product-template duplex in the RdRp core that is ultimately responsible for shunting the ENDO and CBD back into their late-stage elongation positions (Figures 2B and 6).

The determination of several transcription-specific state structures for the SFTSV L proteins allows to make comparisons to LACV L protein, the only other bunyavirus L protein for which transcription-state structures are available so far (32). In LACV, transcription initiation depends on a closure of the C-terminal region and major repositioning of the N-terminal ENDO. These conformational changes were suggested to prompt primer cleavage and primer entry into the RdRp core (39). While transcription initiation in SFTSV also includes a significant repositioning of the N-terminal ENDO, we observe that the C-terminal CBD is also highly mobile. There are therefore differences in how the L proteins from different bunyavirus families enable viral genome replication and transcription.

In our previously published LATE-ELONGATION state structure, although we could fit the CBD with confidence, the cap-binding site was blocked by an arginine blocking motif composed of residues T1838 – V1844 as also observed by others (54–56). In the TRANSCRIPTION-PRIMING and TRANSCRIPTION-EARLY-ELONGATION structures shown here, the blocking motif has been displaced by the capped RNA and now sits orthogonally to the CBD. Interestingly, whereas in the genome replication-related LATE-ELONGATION structure, this arginine motif presumably blocks access to the cap-binding site, in our TRANSCRIPTION-PRIMING and TRANSCRIPTION-EARLY-ELONGATION structures, the residues composing the blocking motif form a wall directing bound capped RNA towards the RdRp core. This is a nice example of multifunctionality, a quintessential feature of the bunyavirus multidomain L protein, which itself is responsible for enabling not just viral genome replication but also transcription.

The capped RNA is bound in principle as we expected with the m^7GTP cap moiety sandwiched between two aromatic

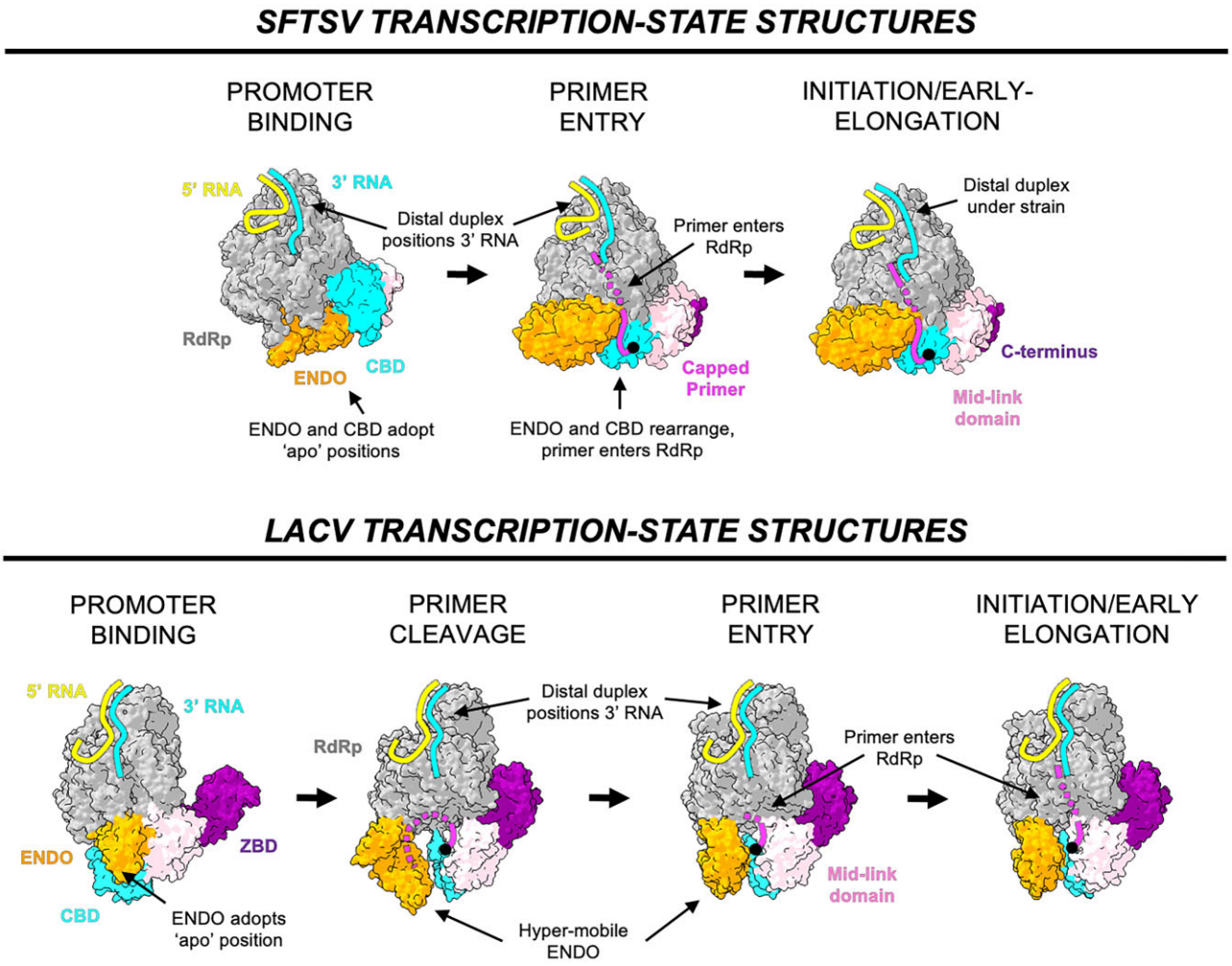

Figure 6. Structure-based models of SFTSV and LACV transcription. L protein structures are displayed as surface with key domains coloured according to the following colour scheme: endonuclease (orange), cap-binding domain (cyan), mid-link domain (light pink), and C terminus (purple). In LACV, the C terminus is the zinc-binding domain (ZBD). The remaining protein is coloured grey. RNAs are represented by coloured solid/dashed lines and coloured either yellow (5′ RNA), cyan (3′ RNA), magenta (product/primer RNA). Key features are indicated. This process overview only includes states with known structural evidence for phenuiviruses and peribunyaviruses and therefore misses some steps such as primer-cleavage and termination.

sidechains: F1703 and Y1719 (Figure 2D). This follows nicely the mode of recognition seen in the crystal structure of the isolated SFTSV CBD bound to m^7GTP cap-analog (18). What is of particular interest, however, is the coordination of nts downstream of the cap. The majority of sidechains supporting the coordination of the capped RNA fragment come from other domains than the CBD. Further, most sidechains interacted with the capped RNA *via* its phosphate backbone rather than with the nt base. This would indicate to us that capped RNA is bound by the L protein regardless of the exact sequence although we cannot exclude that the size of the base (purine vs. pyrimidine) may have an impact.

That being said, the capped RNA used in these experiments was modified by the addition of a cap^0 structure. However, in cells, the most abundant cap structure is cap^1, in which the first nt downstream of the m^7GTP cap is additionally methylated (CH_3) at the 2′-O position of the ribose (57,58). In our TRANSCRIPTION-PRIMING and TRANSCRIPTION-EARLY-ELONGATION structures, a 2′-O methyl group would be prohibitively close to the sidechain of R1851 and the base of the next RNA nt, which in our structures is an A (Supplementary Figure S12). This methyl/base clash would be less severe however, and perhaps not prohibitive at all, if the next base was smaller, *i.e.*, a pyrimidine. Thus, for coordination of cap^1-RNA, there may be a certain degree of sequence specificity or at least preference for a specific set of bases at position 2 after the m^7GTP in the RNA sequence. Interestingly, a preference for smaller bases at this position was found in sequencing data of viral transcripts for the closely-related RVFV. In this case, it has been shown that the L protein preferentially snatches 5′-TOP mRNAs, which have a > 75% chance of containing a pyrimidine at position 2 after the m^7GTP (59). Of course, it is also possible that the R1851 sidechain rotates away from the bound capped RNA and in doing so creates space for the cap^1 methyl group (Supplementary Figure S12). Flexibility in the RNA phosphate backbone may also provide a perfectly sensible solution to this problem. Further work is certainly needed to test these hypotheses and make any concrete proposals regarding the underlying molecular mechanism.

This does not mean however that the ENDO cannot impose some degree of sequence specificity downstream of the cap structure by virtue of preferentially binding and then cleaving specific RNA sequences or motifs. Indeed, it has previ-

ously been proposed based on biochemical studies that the phenuivirus endonuclease prefers purine-rich RNA species as substrates (25). Structural evidence lending weight to this argument is however lacking. Indeed, it would make sense for the ENDO to preferentially cleave at positions producing capped fragments ending in AC as this would then allow the capped fragment to base-pair with the SFTSV 3′ genome termini, which end with UG repeats. That being said, we do not see any strong evidence to suggest that the SFTSV L protein ENDO has a sequence specificity. There is a general lack of structural data showing the SFTSV ENDO bound to an RNA substrate. The only example of this can be found in our previously published LATE-ELONGATION structure, in which we show excess 5′ RNA bound across the ENDO active site. Even here, we could not identify any clear structural determinants that would indicate the ENDO would produce fragments ending in, for example, AC. Although we did speculate that perhaps residue Y76 may make the coordination of a bulky purine base in the equivalent of the P0 pocket (using influenza virus endonuclease nomenclature) less favorable.

Considering the important role the ENDO plays in the cap-snatching process, understanding how the ENDO is regulated is of particular interest. In a previously published structure, our EARLY-ELONGATION-ENDO structure, we demonstrated that the '*raised*' conformation adopted by the ENDO could be one example of such regulatory mechanism. In this conformation, access to the active site is effectively blocked by the positioning of the C-terminal α-helix of the SFTSV ENDO (residues 211–233) across the ENDO active site. Other bunyaviruses have been shown to adopt several different mechanisms for regulating their ENDO domain adding layers of redundancy and complexity to the ENDO regulation. For example, the LASV ENDO has been shown to be autoinhibited by two alternative mechanisms: either an inhibitory peptide or the C-terminal helix of the ENDO blocks the ENDO active site (33). In our TRANSCRIPTION-PRIMING and TRANSCRIPTION-EARLY-ELONGATION structures described here, we find that the C-terminal α-helix of the SFTSV ENDO blocks substrate access to the ENDO active site, albeit in a different way to that seen in the EARLY-ELONGATION-ENDO structure. We have therefore observed the SFTSV ENDO in three unique positions (Supplementary Figure S4) and likely have identified two different mechanisms by which the access to the SFTSV ENDO active site is regulated.

Altogether, the biochemical and structural data provided here give a first glimpse into how the SFTSV L protein likely recognizes and binds to capped RNA fragments in infected cells. We show that the L protein reorganizes its N- and C-terminal domains significantly to present snatched fragments to the RdRp core. This demonstrates, quite unexpectedly, that this priming conformation is retained in the early stages of primer elongation meaning that the L protein adopts very different conformations at early elongation for viral genome replication and transcription. Future work will be needed to elucidate further steps of the viral genome replication and transcription mechanisms, such as termination. Nevertheless, by integrating the now quite significant number of high-resolution cryo-EM structures of the SFTSV L protein undergoing both genome replication and transcription with biochemical data and significant mutational analyses, we can build a more complete picture of how these processes are enabled at the molecular level (Figure 6).

Data availability

Coordinates and maps included in this paper have been deposited in the Worldwide Protein Data Bank (wwPDB) and the Electron Microscopy Data Bank (EMDB) with the following accession codes: SFTSV L protein in a transcription priming state with CBD bound to capped-RNA [TRANSCRIPTION-PRIMING] EMD-18967 PDB-8R6W; SFTSV L protein captured at early elongation following capped-primer incorporation [TRANSCRIPTION-EARLY-ELONGATION] EMD-18969 PDB-8R7Y; SFTSV L protein in a state reflecting cap-independent transcription priming [TRANSCRIPTION-PRIMING (*in vitro*)] EMD-18963 PDB-8R6U. Separately, we have uploaded all uncropped blots and gels to the open repository Zenodo, and the files can be accessed at the following DOI: 10.5281/zenodo.10932309.

Supplementary data

Supplementary Data are available at NAR Online.

Acknowledgements

We want to thank Stephan Günther for his support and helpful discussions throughout the project. We acknowledge support by Carolin Seuring, Cornelia Cazey and Ulrike Laugks for access to the CryoEM multi-user Facility at CSSB and providing time for sample preparation, screening, and data collection; Wolfgang Lugmayr for help and support in using the CSSB partition on the DESY computer cluster for cryo-EM data processing. We also want to thank Lennart Sänger for feedback on the manuscript. Finally, we thank the Wilhelm und Maria Kirmser-Stiftung for support. We thank Dr. Chris Hoffmann for drawing the graphical abstract.

Funding

Leibniz Association's Leibniz competition programme [K72/2017]; part of this work was performed at the cryo-EM multi-user facility at CSSB, headed by K.G. and supported by the UHH and DFG [INST 152/772-1, 774-1, 775-1, 776-1]; in the framework of this project, S.T. benefited from a travel grant from the Leibniz Institute of Virology; E.R.J.Q. was supported by an individual fellowship from the Alexander von Humboldt Foundation and a Klaus Tschira Boost Fund; M.R. received funding from the German Federal Ministry for Education and Research [01KI2019]. Funding for open access charge: Leibniz Association.

Conflict of interest statement

None declared.

References

1. Casel,M.A., Park,S.J. and Choi,Y.K. (2021) Severe fever with thrombocytopenia syndrome virus: emerging novel phlebovirus and their control strategy. *Exp. Mol. Med.*, **53**, 713–722.
2. Kim,K.H., Yi,J., Kim,G., Choi,S.J., Jun,K.I., Kim,N.H., Choe,P.G., Kim,N.J., Lee,J.K. and Oh,M.D. (2013) Severe fever with thrombocytopenia syndrome, South Korea, 2012. *Emerg. Infect. Dis.*, **19**, 1892–1894.
3. Takahashi,T., Maeda,K., Suzuki,T., Ishido,A., Shigeoka,T., Tominaga,T., Kamei,T., Honda,M., Ninomiya,D., Sakai,T., *et al.*

(2014) The first identification and retrospective study of Severe Fever with Thrombocytopenia Syndrome in Japan. *J. Infect. Dis.*, **209**, 816–827.
4. Tran,X.C., Yun,Y., Van An,L., Kim,S.H., Thao,N.T.P., Man,P.K.C., Yoo,J.R., Heo,S.T., Cho,N.H. and Lee,K.H. (2019) Endemic severe fever with thrombocytopenia syndrome, Vietnam. *Emerg. Infect. Dis.*, **25**, 1029–1031.
5. Win,A.M., Nguyen,Y.T.H., Kim,Y., Ha,N.Y., Kang,J.G., Kim,H., San,B., Kyaw,O., Htike,W.W., Choi,D.O., *et al.* (2020) Genotypic heterogeneity of Orientia tsutsugamushi in scrub typhus patients and thrombocytopenia syndrome co-infection, Myanmar. *Emerg. Infect. Dis.*, **26**, 1878–1881.
6. Yu,X.J., Liang,M.F., Zhang,S.Y., Liu,Y., Li,J.D., Sun,Y.L., Zhang,L., Zhang,Q.F., Popov,V.L., Li,C., *et al.* (2011) Fever with thrombocytopenia associated with a novel bunyavirus in China. *N. Engl. J. Med.*, **364**, 1523–1532.
7. Daengnoi,C., Ongkittikul,S., Watanawong,R. and Rompho,P. (2020) Severe fever with thrombocytopenia syndrome virus: the first case report in Thailand. *Bangkok Med. J.*, **16**, 204–206.
8. Huang,X.Y., Du,Y.H., Wang,H.F., You,A.G., Li,Y., Su,J., Nie,Y.F., Ma,H.X. and Xu,B.L. (2019) Prevalence of severe fever with thrombocytopenia syndrome virus in animals in Henan Province, China. *Infect. Dis. Poverty*, **8**, 56.
9. Li,Z., Hu,J., Bao,C., Li,P., Qi,X., Qin,Y., Wang,S., Tan,Z., Zhu,Y., Tang,F., *et al.* (2014) Seroprevalence of antibodies against SFTS virus infection in farmers and animals, Jiangsu, China. *J. Clin. Virol.*, **60**, 185–189.
10. Niu,G., Li,J., Liang,M., Jiang,X., Jiang,M., Yin,H., Wang,Z., Li,C., Zhang,Q., Jin,C., *et al.* (2013) Severe fever with thrombocytopenia syndrome virus among domesticated animals, China. *Emerg. Infect. Dis.*, **19**, 756–763.
11. Yu,M.A., Yu,K.M., Park,S.J., Kim,Y.I., Robles,N.J., Si,Y.J., Kim,E.H., Kwon,H.I., Jeong,H.W., Song,M.S., *et al.* (2019) Seroprevalence of severe fever with thrombocytopenia syndrome phlebovirus in domesticated deer in South Korea. *Virol. Sin.*, **34**, 501–507.
12. Hu,Y.Y., Zhuang,L., Liu,K., Sun,Y., Dai,K., Zhang,X.A., Zhang,P.H., Feng,Z.C., Li,H. and Liu,W. (2020) Role of three tick species in the maintenance and transmission of severe fever with thrombocytopenia syndrome virus. *PLoS Negl. Trop. Dis.*, **14**, e0008368.
13. Luo,L.M., Zhao,L., Wen,H.L., Zhang,Z.T., Liu,J.W., Fang,L.Z., Xue,Z.F., Ma,D.Q., Zhang,X.S., Ding,S.J., *et al.* (2015) Haemaphysalis longicornis ticks as reservoir and vector of severe fever with thrombocytopenia syndrome virus in China. *Emerg. Infect. Dis.*, **21**, 1770–1776.
14. Sun,Y., Li,J., Gao,G.F., Tien,P. and Liu,W. (2018) Bunyavirales ribonucleoproteins: the viral replication and transcription machinery. *Crit. Rev. Microbiol.*, **44**, 522–540.
15. Reguera,J., Gerlach,P., Rosenthal,M., Gaudon,S., Coscia,F., Gunther,S. and Cusack,S. (2016) Comparative structural and functional analysis of bunyavirus and arenavirus Cap-snatching endonucleases. *PLoS Pathog.*, **12**, e1005636.
16. Arragain,B., Effantin,G., Gerlach,P., Reguera,J., Schoehn,G., Cusack,S. and Malet,H. (2020) Pre-initiation and elongation structures of full-length La Crosse virus polymerase reveal functionally important conformational changes. *Nat. Commun.*, **11**, 3590.
17. Vogel,D., Rosenthal,M., Gogrefe,N., Reindl,S. and Gunther,S. (2019) Biochemical characterization of the Lassa virus L protein. *J. Biol. Chem.*, **294**, 8088–8100.
18. Vogel,D., Thorkelsson,S.R., Quemin,E.R.J., Meier,K., Kouba,T., Gogrefe,N., Busch,C., Reindl,S., Gunther,S., Cusack,S., *et al.* (2020) Structural and functional characterization of the severe fever with thrombocytopenia syndrome virus L protein. *Nucleic Acids Res.*, **48**, 5749–5765.
19. Williams,H.M., Thorkelsson,S.R., Vogel,D., Milewski,M., Busch,C., Cusack,S., Grunewald,K., Quemin,E.R.J. and Rosenthal,M. (2023) Structural insights into viral genome replication by the severe fever with thrombocytopenia syndrome virus L protein. *Nucleic Acids Res.*, **51**, 1424–1442.
20. Olschewski,S., Cusack,S. and Rosenthal,M. (2020) The Cap-snatching mechanism of bunyaviruses. *Trends Microbiol.*, **28**, 293–303.
21. Meyer,B.J. and Southern,P.J. (1993) Concurrent sequence analysis of 5′ and 3′ RNA termini by intramolecular circularization reveals 5′ nontemplated bases and 3′ terminal heterogeneity for lymphocytic choriomeningitis virus mRNAs. *J. Virol.*, **67**, 2621–2627.
22. Collett,M.S. (1986) Messenger RNA of the M segment RNA of Rift Valley fever virus. *Virology*, **151**, 151–156.
23. Fernandez-Garcia,Y., Reguera,J., Busch,C., Witte,G., Sanchez-Ramos,O., Betzel,C., Cusack,S., Gunther,S. and Reindl,S. (2016) Atomic structure and biochemical characterization of an RNA endonuclease in the N terminus of Andes virus L protein. *PLoS Pathog.*, **12**, e1005635.
24. Gogrefe,N., Reindl,S., Gunther,S. and Rosenthal,M. (2019) Structure of a functional cap-binding domain in Rift Valley fever virus L protein. *PLoS Pathog.*, **15**, e1007829.
25. Jones,R., Lessoued,S., Meier,K., Devignot,S., Barata-Garcia,S., Mate,M., Bragagnolo,G., Weber,F., Rosenthal,M. and Reguera,J. (2019) Structure and function of the Toscana virus cap-snatching endonuclease. *Nucleic Acids Res.*, **47**, 10914–10930.
26. Morin,B., Coutard,B., Lelke,M., Ferron,F., Kerber,R., Jamal,S., Frangeul,A., Baronti,C., Charrel,R., de Lamballerie,X., *et al.* (2010) The N-terminal domain of the arenavirus L protein is an RNA endonuclease essential in mRNA transcription. *PLoS Pathog.*, **6**, e1001038.
27. Reguera,J., Gerlach,P., Rosenthal,M., Gaudon,S., Coscia,F., Gunther,S. and Cusack,S. (2016) Comparative structural and functional analysis of bunyavirus and arenavirus Cap-snatching endonucleases. *PLoS Pathog.*, **12**, e1005636.
28. Reguera,J., Weber,F. and Cusack,S. (2010) Bunyaviridae RNA polymerases (L-protein) have an N-terminal, influenza-like endonuclease domain, essential for viral Cap-dependent transcription. *PLoS Pathog.*, **6**, e1001101.
29. Rosenthal,M., Gogrefe,N., Vogel,D., Reguera,J., Rauschenberger,B., Cusack,S., Gunther,S. and Reindl,S. (2017) Structural insights into reptarenavirus cap-snatching machinery. *PLoS Pathog.*, **13**, e1006400.
30. Wallat,G.D., Huang,Q., Wang,W., Dong,H., Ly,H., Liang,Y. and Dong,C. (2014) High-resolution structure of the N-terminal endonuclease domain of the Lassa virus L polymerase in complex with magnesium ions. *PLoS One*, **9**, e87577.
31. Wang,W., Shin,W.J., Zhang,B., Choi,Y., Yoo,J.S., Zimmerman,M.I., Frederick,T.E., Bowman,G.R., Gross,M.L., Leung,D.W., *et al.* (2020) The Cap-snatching SFTSV endonuclease domain is an antiviral target. *Cell Rep.*, **30**, 153–163.
32. Arragain,B., Durieux Trouilleton,Q., Baudin,F., Provaznik,J., Azevedo,N., Cusack,S., Schoehn,G. and Malet,H. (2022) Structural snapshots of La Crosse virus polymerase reveal the mechanisms underlying Peribunyaviridae replication and transcription. *Nat. Commun.*, **13**, 902.
33. Kouba,T., Vogel,D., Thorkelsson,S.R., Quemin,E.R.J., Williams,H.M., Milewski,M., Busch,C., Gunther,S., Grunewald,K., Rosenthal,M., *et al.* (2021) Conformational changes in Lassa virus L protein associated with promoter binding and RNA synthesis activity. *Nat. Commun.*, **12**, 7018.
34. Peng,R.C., Xu,X., Jing,J.M., Wang,M., Peng,Q., Liu,S., Wu,Y., Bao,X.C., Wang,P.Y., Qi,J.X., *et al.* (2020) Structural insight into arenavirus replication machinery. *Nature*, **579**, 615.
35. Meier,K., Thorkelsson,S.R., Durieux Trouilleton,Q., Vogel,D., Yu,D., Kosinski,J., Cusack,S., Malet,H., Grunewald,K., Quemin,E.R.J., *et al.* (2023) Structural and functional characterization of the Sin Nombre virus L protein. *PLoS Pathog.*, **19**, e1011533.
36. Durieux Trouilleton,Q., Barata-Garcia,S., Arragain,B., Reguera,J. and Malet,H. (2023) Structures of active Hantaan virus

polymerase uncover the mechanisms of Hantaviridae genome replication. *Nat. Commun.*, **14**, 2954.
37. Keown,J.R., Carrique,L., Nilsson-Payant,B., Fodor,E. and Grimes,J.M. (2023) Structural characterization of the full-length Hantaan virus polymerase. bioRxiv doi: https://doi.org/10.1101/2023.06.09.544421, 09 June 2023, preprint: not peer reviewed.
38. Durieux Trouilleton,Q., Housset,D., Tarillon,P., Arragain,B. and Malet,H. (2024) Structural characterization of the oligomerization of full-length Hantaan virus polymerase into symmetric dimers and hexamers. *Nat. Commun.*, **15**, 2256.
39. Malet,H., Williams,H.M., Cusack,S. and Rosenthal,M. (2023) The mechanism of genome replication and transcription in bunyaviruses. *PLoS Pathog.*, **19**, e1011060.
40. te Velthuis,A.J.W., Robb,N.C., Kapanidis,A.N. and Fodor,E. (2016) The role of the priming loop in influenza A virus RNA synthesis. *Nat. Microbiol.*, **1**, 16029.
41. Wandzik,J.M., Kouba,T., Karuppasamy,M., Pflug,A., Drncova,P., Provaznik,J., Azevedo,N. and Cusack,S. (2020) A structure-based model for the complete transcription cycle of influenza polymerase. *Cell*, **181**, 877–893.
42. Fitzgerald,D.J., Berger,P., Schaffitzel,C., Yamada,K., Richmond,T.J. and Berger,I. (2006) Protein complex expression by using multigene baculoviral vectors. *Nat. Methods*, **3**, 1021–1032.
43. Bieniossek,C., Imasaki,T., Takagi,Y. and Berger,I. (2012) MultiBac: expanding the research toolbox for multiprotein complexes. *Trends Biochem. Sci.*, **37**, 49–57.
44. Jerome,H., Rudolf,M., Lelke,M., Pahlmann,M., Busch,C., Bockholt,S., Wurr,S., Gunther,S., Rosenthal,M. and Kerber,R. (2019) Rift Valley fever virus minigenome system for investigating the role of L protein residues in viral transcription and replication. *J. Gen. Virol.*, **100**, 1093–1098.
45. Kimanius,D., Dong,L., Sharov,G., Nakane,T. and Scheres,S.H.W. (2021) New tools for automated cryo-EM single-particle analysis in RELION-4.0. *Biochem. J.*, **478**, 4169–4185.
46. Zheng,S.Q., Palovcak,E., Armache,J.P., Verba,K.A., Cheng,Y. and Agard,D.A. (2017) MotionCor2: anisotropic correction of beam-induced motion for improved cryo-electron microscopy. *Nat. Methods*, **14**, 331–332.
47. Tegunov,D. and Cramer,P. (2019) Real-time cryo-electron microscopy data preprocessing with Warp. *Nat. Methods*, **16**, 1146–1152.
48. Mindell,J.A. and Grigorieff,N. (2003) Accurate determination of local defocus and specimen tilt in electron microscopy. *J. Struct. Biol.*, **142**, 334–347.
49. Emsley,P., Lohkamp,B., Scott,W.G. and Cowtan,K. (2010) Features and development of Coot. *Acta. Crystallogr. D Biol. Crystallogr.*, **66**, 486–501.
50. Afonine,P.V., Poon,B.K., Read,R.J., Sobolev,O.V., Terwilliger,T.C., Urzhumtsev,A. and Adams,P.D. (2018) Real-space refinement in PHENIX for cryo-EM and crystallography. *Acta Crystallogr D Struct Biol*, **74**, 531–544.
51. Williams,C.J., Headd,J.J., Moriarty,N.W., Prisant,M.G., Videau,L.L., Deis,L.N., Verma,V., Keedy,D.A., Hintze,B.J., Chen,V.B., *et al.* (2018) MolProbity: more and better reference data for improved all-atom structure validation. *Protein Sci.*, **27**, 293–315.
52. McNicholas,S., Potterton,E., Wilson,K.S. and Noble,M.E. (2011) Presenting your structures: the CCP4mg molecular-graphics software. *Acta. Crystallogr. D Biol. Crystallogr.*, **67**, 386–394.
53. Pettersen,E.F., Goddard,T.D., Huang,C.R.C., Meng,E.E.C., Couch,G.S., Croll,T.I., Morris,J.H. and Ferrin,T.E. (2021) UCSF ChimeraX: structure visualization for researchers, educators, and developers. *Protein Sci.*, **30**, 70–82.
54. Wang,P., Liu,L., Liu,A. and Lou,Z. (2021) Reply to: errors in the deposited SFTSV L protein structure. *Nat. Microbiol.*, **6**, 551–552.
55. Wang,P., Liu,L., Liu,A., Yan,L., He,Y., Shen,S., Hu,M., Guo,Y., Liu,H., Liu,C., *et al.* (2020) Structure of severe fever with thrombocytopenia syndrome virus L protein elucidates the mechanisms of viral transcription initiation. *Nat. Microbiol.*, **5**, 864–871.
56. Cusack,S. and Rosenthal,M. (2021) Errors in the deposited SFTSV L protein structure. *Nat. Microbiol.*, **6**, 549–550.
57. Furuichi,Y. (2015) Discovery of m(7)G-cap in eukaryotic mRNAs. *Proc. Jpn Acad Ser. B Phys. Biol. Sci.*, **91**, 394–409.
58. Shatkin,A.J. (1976) Capping of eucaryotic mRNAs. *Cell*, **9**, 645–653.
59. Hopkins,K.C., Tartell,M.A., Herrmann,C., Hackett,B.A., Taschuk,F., Panda,D., Menghani,S.V., Sabin,L.R. and Cherry,S. (2015) Virus-induced translational arrest through 4EBP1/2-dependent decay of 5′-TOP mRNAs restricts viral infection. *Proc. Natl. Acad. Sci. U.S.A.*, **112**, E2920–E2929.

Received: December 18, 2023. **Revised:** April 10, 2024. **Editorial Decision:** April 11, 2024. **Accepted:** April 19, 2024